



CHORUS

This is the accepted manuscript made available via CHORUS. The article has been published as:

Intra-unit-cell magnetic order in stoichiometric $\text{La}_{2}\text{CuO}_{4}$

Vyacheslav G. Storchak, Jess H. Brewer, Dmitry G. Eshchenko, Patrick W. Mengyan, Oleg E. Parfenov, Andrey M. Tokmachev, Pinder Dosanjh, and Sergey N. Barilo

Phys. Rev. B **91**, 205122 — Published 21 May 2015

DOI: [10.1103/PhysRevB.91.205122](https://doi.org/10.1103/PhysRevB.91.205122)

Intra-unit-cell Magnetic Order in Stoichiometric La_2CuO_4

Vyacheslav G. Storchak,^{1,*} Jess H. Brewer,² Dmitry G. Eshchenko,³ Patrick W. Mengyan,⁴
Oleg E. Parfenov,¹ Andrey M. Tokmachev,¹ Pinder Dosanjh,² and Sergey N. Barilo⁵

¹*National Research Centre “Kurchatov Institute”, Kurchatov Sq. 1, Moscow 123182, Russia*

²*Department of Physics and Astronomy, University of British Columbia, Vancouver, BC, Canada V6T 1Z1*

³*Bruker BioSpin AG, Industriestrasse 26, 8117 Fällanden, Switzerland*

⁴*Department of Physics, Texas Tech University, Lubbock, Texas 79409-1051, USA*

⁵*Institute of Solid State and Semiconductor Physics, Minsk 220072, Belarus*

(Dated: 5 May 2015)

Muon spin rotation measurements, supported by magnetization experiments, have been carried out in a stoichiometric high- T_c parent compound La_2CuO_4 in a temperature range from 2 K to 340 K and in transverse magnetic fields up to 5 T. Along with the antiferromagnetic local field, muon spin rotation spectra indicate presence of an additional source of magnetic field on the muon. The characteristic splitting of about 45 G, coming from this additional magnetic field, is consistent with spontaneous circulating currents model of Varma.

PACS numbers: 74.72.Cj, 75.45.+j, 75.50.Ee, 76.75.+i

I. INTRODUCTION

The idea of a pseudogap (PG) has recently played a key role in our understanding of strongly correlated electron systems — particularly those exhibiting high- T_c superconductivity (SC). Although some basic phenomenology of copper oxide superconductors — electron pairs with nonzero angular momentum, an exchange mechanism arising from strong Coulomb interaction between the valence electrons, and a remarkable departure from the Fermi liquid behavior in the normal state — is a matter of growing consensus, the microscopic mechanism still remains unclear. Understanding the origin of the PG and its relation to high- T_c SC is considered an important step towards revealing this mechanism¹⁻³.

All these cuprates, being hole (p) doped, have the same T-p phase diagram: at zero doping they are antiferromagnetic (AFM) Mott insulators while doping easily destroys the AFM and makes the system metallic. In the overdoped regime, the normal state exhibits properties of a correlated Fermi liquid. By contrast, in the underdoped regime, cuprates show features of a correlated metal exhibiting non-Fermi-liquid behavior. Their transport, magnetic and thermodynamic properties point towards strong reduction of the electronic density of states (DOS) below a temperature T^* , although the DOS does not reach zero at the lowest temperature and the system remains metallic¹ — hence the PG terminology. Angle-resolved photoemission spectroscopy (ARPES)⁴ suggests opening of a real gap in the one-particle excitation spectrum, supported by other spectroscopic techniques³.

As doping dependence of the SC gap follows T^* rather than T_c , the PG has been considered as a precursor to the SC gap; the PG phase being a *disordered* state with broken phase coherence among preformed pairs, which condense below T_c as soon as phase coherence is established⁵. A different approach considers the PG state as an *ordered* phase with a well defined order parameter and a related

broken symmetry⁶⁻⁸. In this scenario, T^* is the transition temperature to an ordered PG phase of orbital magnetic moments caused by spontaneous circulating currents (CC). The fluctuations associated with the broken symmetry are considered to be responsible for both the superconductivity, playing role of a pairing glue, and the non-Fermi-liquid behavior below T^* .

To date, ARPES data are rather controversial: an apparent spontaneous dichroism of $\text{Bi}_2\text{Sr}_2\text{CaCu}_2\text{O}_{8+\delta}$ ⁴ indicates a time-reversal symmetry breaking (TRSB) magnetic field in the PG phase — a fingerprint of an ordered state. Such dichroism, however, was not found in a later experiment⁹. The key experimental evidence for a novel ordered state comes from spin-polarized neutron scattering experiments, which report commensurate magnetic peaks below T^* in YBCO and $\text{Hg}1201$ ¹⁰⁻¹², pointing to TRSB that, nevertheless, preserves lattice translation invariance, as the nuclear and magnetic peaks in reciprocal space are superimposed on Bragg reflections. Sizeable magnetic moments (on the order of 0.1-0.2 μ_B) are reported in the PG state.

Positive muons, as local microscopic magnetic probes, are especially sensitive to any kind of magnetic order, manifested as a coherent muon spin oscillation with frequency proportional to the local magnetic field at the muon¹³. However, muon spin rotation (μSR) experiments, which have convincingly demonstrated their sensitivity to TRSB fields in a number of weak magnetic systems, produced no evidence of magnetic order in the PG state. At first, spontaneous static magnetic fields were reported in YBCO¹⁴, which were later reinterpreted as being due to spatial charge inhomogeneities¹⁵. No TRSB is reported in $\text{La}_{2-x}\text{Sr}_x\text{CuO}_4$ (for $x=0.13$ and $x=0.19$, both within the PG regime) where μSR experiments set an upper limit of ~ 0.2 G for any magnetic field at the muon site, while the expected TRSB local field is estimated to amount about 40 G¹⁶. This discrepancy between neutron and muon experiments has been attributed to screening

of the charge density in the metallic-plane unit cells in the vicinity of the muon¹⁷.

On the other hand, orbital currents and associated magnetic moments may well be present in the limiting case of the underdoped regime — insulating stoichiometric La_2CuO_4 — should CC be an intimate feature of chemical bonding in the CuO_2 plane. Recent studies of the phase diagram for high- T_c cuprate SC¹⁸ suggest that a large part of the phase diagram (including zero doping limit) is occupied by the loop current phase. Its stability depends much stronger on the charge transfer energy than on hole doping. The estimated charge transfer energy (for $\text{La}_{2-x}\text{Sr}_x\text{CuO}_4$) suggests that the loop current phase can exist at zero doping. Orbital currents are also observed in a copper-oxygen plaquette of AFM cupric oxide¹⁹.

In this paper, we present μSR spectroscopy of stoichiometric La_2CuO_4 , in which the magnetic field at the muon should not be affected by charge density screening. Our data indicate *an additional source of magnetic field* at the muon site (over and above the previously known AFM field) consistent with the model of circulating currents and polarized neutron experiments.

II. THE EXPERIMENT

Single crystals of $\text{La}_2\text{CuO}_{4+x}$ grown from CuO flux are used for these studies. The crystal orientation, lattice parameters and mosaicity (less than 0.05° along the \hat{c} -axis) are determined by X-ray diffractometry. Surplus oxygen is removed by annealing in vacuum. The lattice parameters correspond to the low-temperature orthorhombic stoichiometric La_2CuO_4 ($Bmab$ space group)²⁰. The Néel temperature $T_N = 320$ K is measured by SQUID.

Time-differential μSR experiments, using 100% spin-polarized positive muons, are carried out on the M15 surface muon channel at TRIUMF using the *HiTime* spectrometer. A brief description of the experimental setup is given in Appendix A.

III. EXPERIMENTAL RESULTS

At low temperature, the zero-field (ZF) μSR spectra consist of two components (small and large amplitude), well known from previous studies and indicative of two inequivalent muon sites in AFM La_2CuO_4 . The Néel temperature and magnetic fields at the muon sites $B = 428.7$ G (high-frequency, large amplitude component) and $B = 111.8$ G (low-frequency, small amplitude component)²¹ are consistent with earlier studies.

In high magnetic field H applied transverse to the muon spin polarization and parallel to the \hat{c} -axis of the La_2CuO_4 crystal, μSR spectra exhibit 7 signals (Fig. 1). The frequency of the muon precession for each signal is proportional to the local magnetic field B on the muon: $\nu_\mu = \gamma_\mu B / 2\pi$, where $\gamma_\mu = 2\pi \times 135.53879$ MHz/T is the

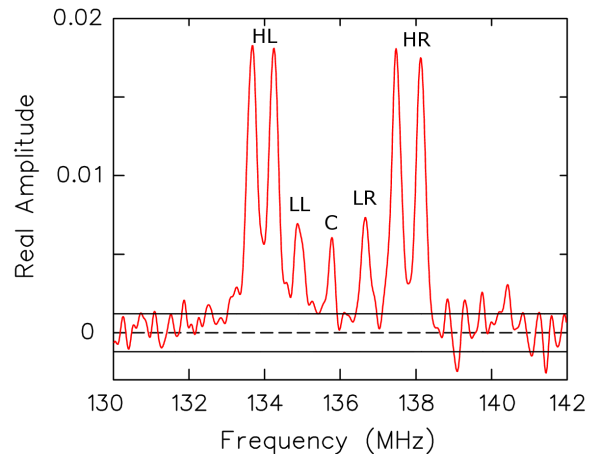


FIG. 1: Frequency spectrum of muon spin precession in AFM stoichiometric La_2CuO_4 in a transverse magnetic field $H = 1$ T directed along the \hat{c} -axis of the crystal at $T = 100$ K. The line C frequency corresponds to the background signal.

muon gyromagnetic ratio. Line C at about 135.6 MHz coincides with the single line detected in CaCO_3 , a non-magnetic reference sample, and originates from muons that miss the sample and stop in a non-magnetic environment. Small peaks LL and LR positioned around the central line correspond to the AFM splitting of the low-frequency signal observed in zero magnetic field. Our main interest is focused on the large-amplitude signals HL and HR positioned symmetrically around the central line. We associate these signals with the high-frequency signal in zero magnetic field. The evolution of μSR spectra with temperature is presented in Fig. 2. A typical time-domain spectrum and a series of spectra with in-plane direction of the external field are provided in the Appendices.

Within the AFM phase, one should expect 4 distinct signals in the high-field μSR spectra from two independent (and distinct) muon sites in the AFM host. Instead, we detect 6 peaks coming from muons stopped in the La_2CuO_4 crystal. Observation of additional peaks in the high-field μSR spectra might point to the formation of spin polarons recently detected in a number of strongly correlated electron materials, both insulating or semiconducting^{22–29} and metallic^{30,31}. However, analysis of the μSR signals' frequencies and amplitudes rules out this interpretation. On the other hand, additional peaks may indicate that, apart from the AFM fields, there is *an additional source of magnetic field on the muon* which causes the characteristic splitting of HL and HR signals (see Figs. 1 and 2). To determine the origin of this field, one needs a detailed interpretation of the μSR spectra based on the muon sites in La_2CuO_4 .

IV. DISCUSSION: STRUCTURAL CONSIDERATIONS

Identification of the muon stopping sites from ZF- μ SR spectra has been discussed by many authors^{32–36}. However, information obtained from ZF spectra alone is insufficient and additional guidance is typically sought from first-principles electronic structure calculations. It is common to predict the muon stopping site to be in the vicinity of the apical oxygen atom, but the muon positions that are actually determined are quite different in a number of studies, which leads to much confusion. In contrast, high-field μ SR measurements, which determine the magnitudes of the *projections* (onto the directions of the applied field; see Appendix B) of the local magnetic field at the muon, provide more precise information on the muon positions in La_2CuO_4 (in combination with ZF data and the known crystal and magnetic structure of the system).

At 530 K the high-temperature tetragonal phase transforms into the orthorhombic phase which doubles the unit cell^{37,38}. This structural transition is due to a rotation of the central CuO_6 octahedra around the tetragonal axes (110) and antiphase rotations of octahedra in the neighbouring unit cells. At low temperature, the tilting of CuO_6 octahedra reaches 5° ³⁷. Stoichiometric La_2CuO_4 is a collinear AFM with four sublattices.

The magnetic moment of a Cu atom amounts to $0.66 \pm 0.13 \mu_B$ and is directed along the diagonal of the CuO_2 plaquette^{37,39}. A peculiar feature of magnetic ordering in La_2CuO_4 is the presence of a weak ($\sim 0.002 \mu_B$ per Cu atom) ferromagnetic coupling of spins within CuO_2 layers^{37,40} possibly originating from Dzyaloshinskii-Moriya exchange interactions and leading

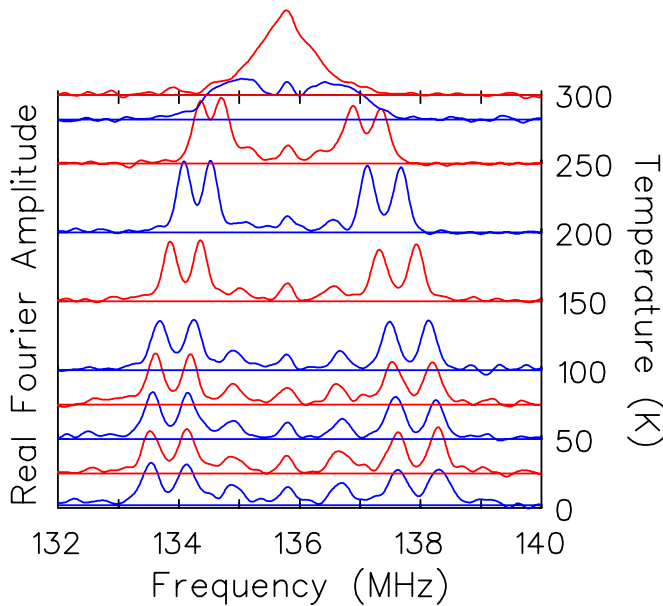


FIG. 2: Fourier transforms of the muon spin precession signal in AFM stoichiometric La_2CuO_4 in an external magnetic field $H = 1$ T directed along the \hat{c} -axis of the crystal at different temperatures.

to a small tilting ($\sim 0.17^\circ$) of Cu magnetic moments^{38,40}. These small moments are orthogonal to CuO_2 layers and have opposite directions in the neighbouring planes. Thus La_2CuO_4 is an antiferromagnet with hidden, weak ferromagnetism.

We determine the muon stopping sites using the dipole-field approximation and assuming the periodic AFM structure of La_2CuO_4 with the known moments on Cu atoms. High-field μ SR spectra were recorded for three different mutually orthogonal orientations of the sample, providing absolute values of the local magnetic field projections at the muon sites. There are two sites: the small-field site gives two peaks LL and LR (one for each direction of the AFM dipolar field); the large-field site gives peaks HL and HR (each split by some additional contribution). Chemically possible muon positions consistent with the μ SR data are shown in Appendix B. The picture is quite simple: the muon is bound to an apical oxygen atom, but it can be located on the side closer to a Cu atom (signal with higher ZF frequency) or the other side, closer to a La atom (signal with lower ZF frequency).

The muon is located somewhat closer to the oxygen atom than expected from the typical O-H bond distance of ~ 1 Å. This can be explained by a small perturbation of the loosely bound apical oxygen position due to its bonding with the muon. A significant disturbance of the system by the muon itself is unlikely because the Néel temperature determined from zero-field μ SR experiments coincides with that measured by SQUID. Other corrections (*e.g.* uncertainty in the value of the magnetic moment on Cu and approximations of the computational procedure) are estimated to be small and therefore insignificant to the general conclusions.

The magnetic fields are almost indifferent to the tilting of CuO_6 octahedra because the canted component of the moment on Cu is very small. Nevertheless, the tilting produces two types of structurally inequivalent positions for muons differing in the distance between the muon and the apical oxygen. However, the choice between them does not affect our conclusions.

The observed splittings cannot be explained by inequivalent muon sites arising from tilting of CuO_6 octahedra: The proof is provided by a spin-flop transition in high magnetic field applied along the \hat{c} -axis^{38,40}. As a result, the direction of small ferromagnetic moments in every CuO_2 plane becomes the same. This change is accompanied by reversal of in-plane components of magnetic moments for every second CuO_2 plane. At $T = 250$ K, SQUID measurements show that a spin-flop transition occurs at $H \sim 4$ T²¹. The jump of magnetization is consistent with the literature data^{38,40}. This spin-flop transition is detected at 250 K (Fig. 3) where lines LR and HR in the μ SR spectra vanish in high magnetic field. Such a transition makes the magnetic unit cell equivalent to the crystallographic unit cell and the number of magnetic sublattices decreases from four to two: magnetic structures of neighbouring CuO_2 planes

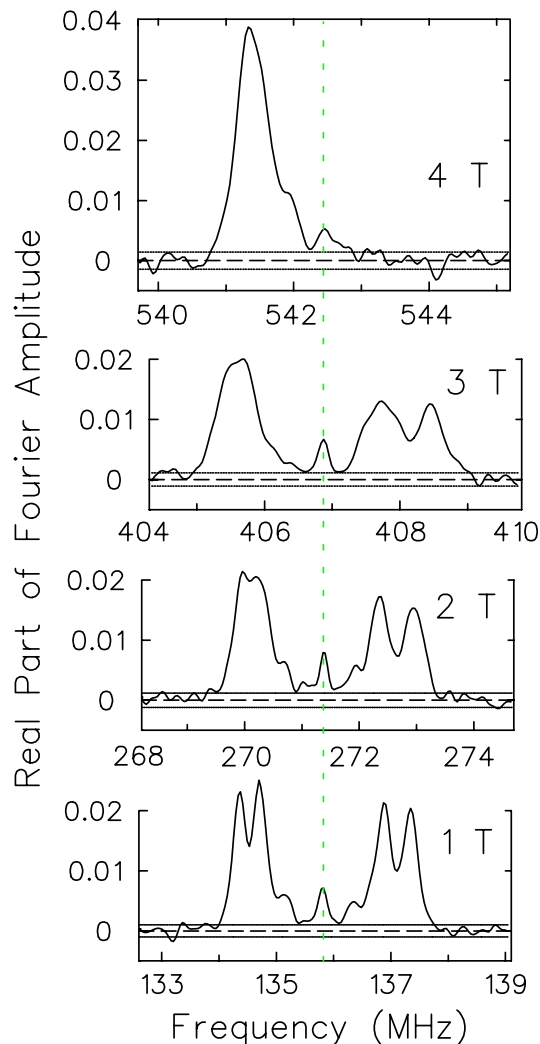


FIG. 3: Fourier transforms of the μ SR signals in AFM stoichiometric La_2CuO_4 at $T = 250$ K in different external magnetic fields directed along the \hat{c} -axis of the crystal.

become equivalent with respect to the tilting of CuO_6 octahedra. The change of the spectra is consistent with the muon stopping at only one side of CuO_6 octahedra and contradicts the hypothesis that the splitting is due to muons stopping at both sides of CuO_6 octahedra.

Then one can try to ascribe the splitting to structural deformations leading to two types of tilted octahedra. Indeed, there are suggestions that a lower symmetry ($Bm11$ space group) is possible, but our calculations show that the proposed structural deformations⁴¹ are more than 3 times smaller than the difference in muon positions required to explain splitting of the lines. Moreover, equal amplitudes of the split signals (Fig. 1) would be a surprising coincidence for different muon stopping sites.

Therefore we conclude that the splittings are due to an additional source of the magnetic field (besides AFM). This field cannot originate from the apical oxygens because it should cause comparable splittings of both low- and high-frequency signals. Instead, the source of this additional magnetic field is likely confined within CuO_2 planes. Then the apparent absence of splittings in LL

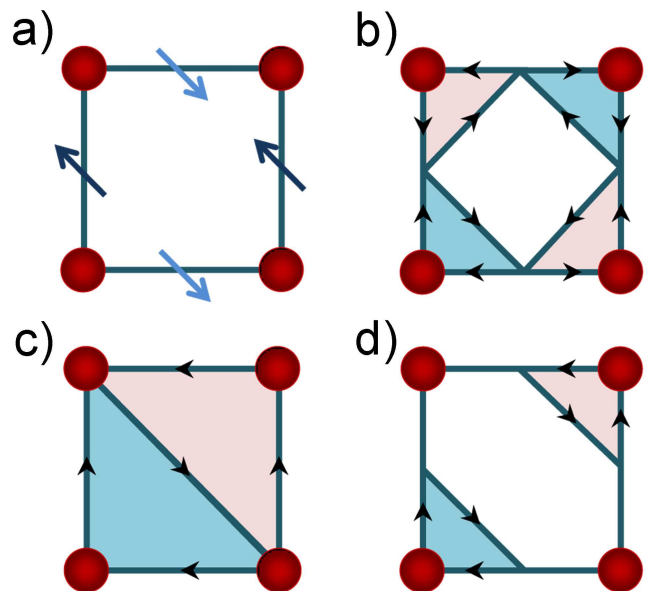


FIG. 4: Proposed sources of magnetic order in La_2CuO_4 : a) AFM order of spins on oxygen atoms; b) $CC-\Theta_I$ model with 4 orbital current loops per CuO_2 plaquette; c) staggered orbital current phase with Cu-Cu-Cu current loops; d) $CC-\Theta_{II}$ model with two opposite current loops O-Cu-O per plaquette.

and LR signals can be easily explained by the increased distance from the muon to CuO_2 planes, leading to much smaller splittings that are not resolved in the experiment.

V. DISCUSSION: MODELS OF THE MAGNETIC ORDER

There are two major types of models explaining intra-unit-cell magnetic order in cuprates. One is based on AFM spin polarization of oxygen atoms (Fig. 4a) while the other relies upon circulating orbital currents. Neutron experiments have not been able to differentiate the existing models beyond establishing TRSB^{10,11}. In contrast, high-field μ SR experiments (in combination with simple symmetry considerations) may provide such differentiation based on the ratio of splittings for different directions of the magnetic field.

The former model of oxygen spins¹⁰ has the correct symmetry structure to describe the splittings, but the ratio of in-plane and out-of-plane splittings, α , is about 1.6, while our experiments give 1.0. More importantly, this model predicts large (~ 40 G) splitting of the high-frequency signal in the absence of magnetic fields, which is not observed in the ZF- μ SR spectra. An alternative model with antiferromagnetic ordering of spins directed along the \hat{c} -axis⁴² has an incorrect symmetry structure since it does not provide splitting of signals for fields along the \hat{c} -axis.

Alternatively, magnetic order can be based on current loops within the unit cell. The original model $CC-\Theta_I$

(Fig. 4b) is formed by 4 orbital current loops O-Cu-O for each CuO_2 plaquette⁶. This model is not consistent with either polarized neutron experiments or our μSR data, as the symmetry of the model prevents the splitting of signals for fields directed along the \hat{c} -axis. An alternative one-band model with staggered orbital current phase formed by Cu-Cu-Cu currents⁴³ (Fig. 4c) has correct symmetry but the calculated ratio α is too large and the absence of splitting in the ZF spectra can not be explained within this model.

The most widely used CC model of intra-unit-cell magnetic order is $CC-\Theta_{II}$ (Fig. 4d) with two opposite current loops O-Cu-O per CuO_2 plaquette⁷. The basic symmetry is correct and the calculated ratio α (~ 1.1) is close to the experimental value. However, this model still provides an incorrect description of ZF- μSR spectra.

Neutron experiments reveal that the moments responsible for the intra-unit-cell magnetic order should be significantly tilted, with a tilting angle $45 \pm 20^\circ$ ^{10,11}. This constitutes a significant departure from the original CC model. However, attempts to reconcile the theory and the experiment have been made based on accounts of spin-orbit interactions⁴⁴ and quantum interference of current loop states⁴⁵. Our calculations show that the correct ratio of splittings is achieved for a tilting of orbital moments by $\sim 53^\circ$ within the $CC-\Theta_{II}$ model. Moreover, this modified model is the only one consistent with zero magnetic field data: the changes of the magnetic field have opposite signs for the in-plane component and that along the \hat{c} -axis; thus the splitting of the ZF signal becomes small and hence not resolved. In other words, the magnetic field vectors on the muon arising from AFM moments and tilted orbital moments are approximately orthogonal. The resulting magnetic fields have approximately the same absolute values and therefore are not resolved in ZF measurements. The orbital moment extracted from our data amounts to about $0.04 \mu_B$, which is comparable with the theoretical value on the order of $0.1 \mu_B$ ⁶. Within this model the splitting of LL and LR signals is indeed small (the actual value depends on the muon position with respect to tilting of CuO_6 octahedra and relative directions of circulating currents in the neighbouring CuO_2 planes).

VI. SUMMARY

High magnetic field μSR studies in orthorhombic La_2CuO_4 reveal an additional source of magnetic field within the unit cell, consistent with the model of circulating currents, though there is no suggestion on our part that this model is the only one consistent with the μSR data.

ACKNOWLEDGMENTS

This work was partially supported by Kurchatov Institute, Russian Science Foundation (Grant 14-19-00662), Russian Foundation for Basic Research (Grant 13-07-00095), NSERC of Canada and the U.S. DOE, Basic Energy Sciences (Grant DE-SC0001769).

Appendix A: μSR SETUP

Transverse field muon spin rotation (TF- μSR) utilizes positively charged, 100% spin polarized muons implanted into a sample where an external magnetic field is applied transverse to the initial spin polarization direction. The time evolution of the μ^+ spin polarization, $P_\mu(t)$, is measured by monitoring positrons emitted preferentially along the μ^+ spin direction, at the time of decay. The raw experimental measure is a positron count, binned by time of decay, that is then used to determine $P_\mu(t)$ by computing, what is effectively, a weighted average of these positron counts in opposing detectors and is therefore a projection of the μ^+ spin on the axis of the existing field direction. Fig. 5 shows a scheme of the experimental setup. A detailed outline of μSR technique is given in¹³.

A typical TF spin polarization function can be modeled in the form

$$P_\mu(t) = \sum_n A_n G_n(t) \cos(\omega_{\mu,n}t + \phi_n) \quad (\text{A1})$$

where the μ^+ in site (or state) n precesses at the Larmor frequency ($\omega_\mu = \gamma_\mu B$) thereby directly probing the net

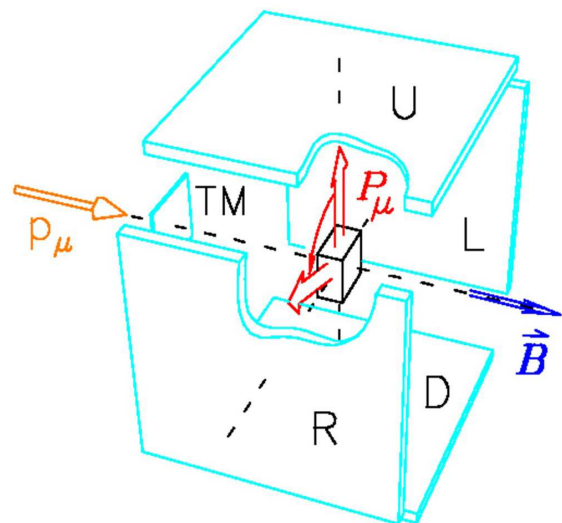


FIG. 5: Experimental setup for TF- μSR experiments. \vec{B} is the external magnetic field; p_μ is the momentum of the muon; P_μ is its spin polarization; U , D , L and R are positron detectors (up, down, left and right); TM is the incident muon counter; the sample is in the center.

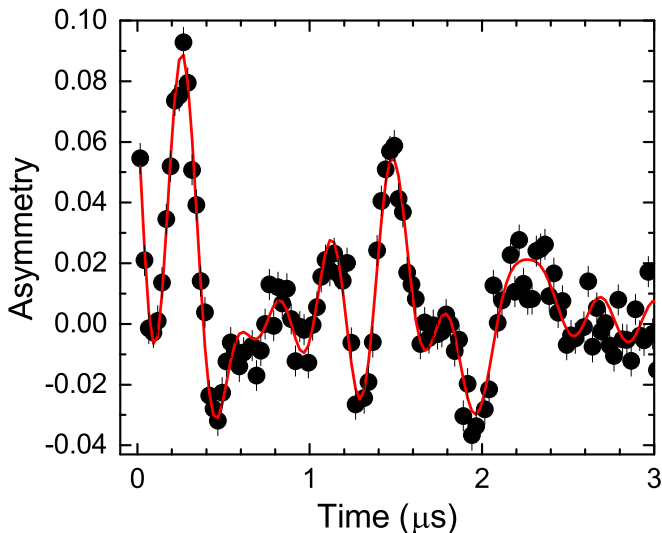


FIG. 6: Time-domain spectrum of muon spin precession in La_2CuO_4 in a transverse magnetic field of $B=1$ T along the \hat{c} -axis at $T=50$ K in a rotating reference frame with frequency 135 MHz. The solid line is a fit based on 7 oscillating components.

local field B of that state. The amplitude A_n is a measure of signal intensity, which directly correlates to the probability of a μ^+ persisting in state n . The relaxation parameter $G_n(t)$ characterizes the way in which the measured time evolution of the precessing signal is damped which relates to the distribution of local fields, inhomogeneity and changes therein. Phase ϕ refers to the apparent shift of the initial μ^+ precession within the spectra typically associated with decoherence of the precession that can be caused by processes such as electron capture or loss. A typical time-domain TF- μ SR spectrum from La_2CuO_4 and its fit for $n = 7$ oscillating components are shown in Fig. 6.

Appendix B: MAGNETIC FIELD CALCULATIONS

The frequency of the muon precession is proportional to the magnetic field B on the muon. Zero field μ SR experiments determine the absolute value of the local magnetic field on the muon. TF- μ SR experiments provide richer information: one can calculate projections of the local magnetic field on the direction of the external magnetic field. The local magnetic field vector has a component B_{\parallel} along the direction of the external magnetic field of amplitude B_{ext} and the orthogonal component B_{\perp} . Then, the amplitude of the field as determined by TF- μ SR is $B = \sqrt{(B_{\parallel} + B_{ext})^2 + B_{\perp}^2}$. The component B_{\parallel} is then $(B^2 - B_0^2 - B_{ext}^2)/2B_{ext}$, where $B_0 = \sqrt{B_{\parallel}^2 + B_{\perp}^2}$ is the amplitude of the local magnetic field as determined by ZF- μ SR. When $B_{ext} \gg B_0$ the approximation $B_{\parallel} \approx B - B_{ext}$ can be used.

Thus, calculation of the components of the local mag-

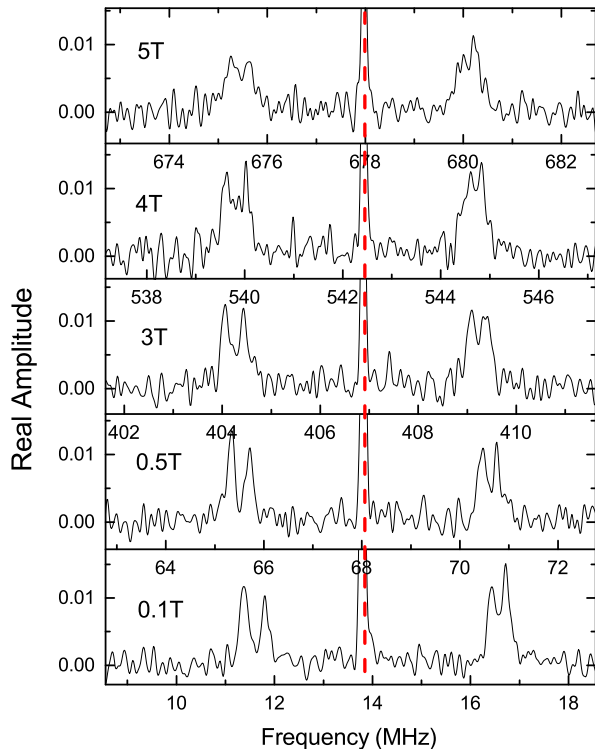


FIG. 7: Fourier transforms of the muon spin precession signal in La_2CuO_4 at $T=250$ K in different transverse magnetic fields ($B=0.1, 0.5, 3, 4, 5$ T) directed along one of in-plane tetragonal axes. The noise is different from that in Fig. 3 due to different run lengths ($10 \mu\text{s}$ vs. $4 \mu\text{s}$ for Fig. 3).

netic field vector requires TF- μ SR studies for different directions of the external magnetic field with respect to the crystalline axes. We performed experiments with the field directed along tetragonal axes of the crystal. TF- μ SR frequency spectra for the external magnetic field directed along the \hat{c} -axis of La_2CuO_4 are shown in Figs. 1-3. Fig. 7 demonstrates the analogous spectrum at $T=250$ K in different magnetic fields directed along one of in-plane tetragonal axes. The spectrum along the other in-plane axis is virtually the same. Equal magnetic field projections along two tetragonal in-plane axes mean that the in-plane component of the magnetic field on the muon is along a diagonal of the plaquette and, according to the Pythagorean theorem, the total in-plane projection is $\sqrt{2}$ times larger than each of the projections along the in-plane tetragonal axes. This total in-plane projection is used in calculating the ratios of in-plane and out-of-plane splittings.

Our experiments provide components of the local magnetic field vectors on the muons for each signal of the spectrum (corresponding to different muon stopping sites). This information can be used to determine the muon stopping sites. There is a plethora of potential sources that may contribute to the local magnetic environment to which the muon is sensitive. However, the lo-

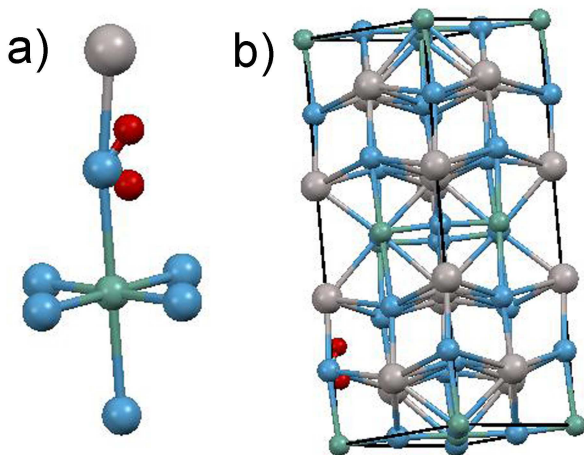


FIG. 8: Muon stopping sites as determined from dipole-field calculations and shown a) with respect to CuO_6 octahedra, b) within $Bmab$ unit cell of La_2CuO_4 (green - Cu, grey - La, blue - O, red - muon positions).

cal magnetic field on the muon is normally dominated by (dipole field) contributions coming from local moments. Each moment \vec{m} produces a dipolar magnetic field:

$$\vec{B}(\vec{r}) = \frac{\mu_0}{4\pi} \left[\frac{3\vec{r}(\vec{m} \cdot \vec{r})}{r^5} - \frac{\vec{m}}{r^3} \right]. \quad (\text{B1})$$

The sum of these contributions from known moments over the entire sample allows for determination of the local magnetic field vector in every point of the crystal. It remains to scan the unit cell and find a set of points where the calculated local magnetic field vector coincides with that determined in the experiment. These points can be considered as possible muon stopping sites. To distinguish between them, external information is typically sought from quantum-mechanical calculations for muons in different crystallographic positions. In the particular case of La_2CuO_4 the absolute values and directions of static magnetic moments are known: there is a large in-plane antiferromagnetic moment on each Cu atom bisecting O-Cu-O angle and a very small out-of-plane component. The procedure using dipole-field calculations is quite standard. It has been previously applied to La_2CuO_4 ^{32,36}. The difference is in the input data. Our TF- μSR experiments determine not only the absolute values of the magnetic fields on the muons but also their projections on the selected directions (as well

as splitting of the signals due to an additional source of magnetic field). Based on these data, we found two possible independent positions for each of the two muon stopping sites. In each case one of the positions can be rejected based on chemical considerations. Figure 8 shows the calculated muon stopping sites consistent with the μSR data.

The calculations do not rule out the possibility of the muon stopping at different sides of the CuO_6 octahedra with respect to their tilting. Luckily, it can be done by observing disappearance of the right half of the lines in the μSR spectra at the spin-flop transition (see Fig. 3).

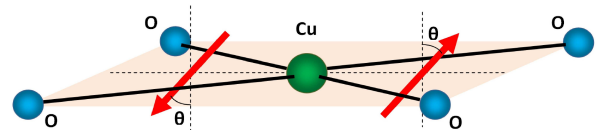


FIG. 9: Tilted orbital moments (red) in the modified model of orbital currents. Angle θ is between the orbital moment and the \hat{c} -axis direction.

The presence of the spin-flop transition is confirmed by SQUID magnetization measurements.

The knowledge of the muon stopping sites allows for analysis of possible models for an additional source of the magnetic field. From the TF- μSR experiments we know the ratio of in-plane and out-of-plane components of the magnetic field which produces additional splitting. Although this is not enough to determine the source of the splitting, it can differentiate between the existing models. The scheme of the calculation is the same. Each model for an additional source of the magnetic field is characterized by a set of magnetic moments in the unit cell. Therefore, one can determine the additional field on the muon (signal splittings) arising from these moments within the dipole-field approximation. The dipole-field calculations for the ratio mentioned above do not depend on the strength of the source of the magnetic field (absolute value of the moments). Based on these calculations we determine that a modified model of circulating orbital currents is consistent with the observed splittings while other models are not. Figure 9 shows orbital moments for this model of orbital currents. This picture of tilted orbital moments is consistent with the spin-polarized neutron scattering data for cuprates^{10,11}.

* Electronic address: mussr@triumf.ca

¹ M. R. Norman and C. Pépin, Rep. Prog. Phys. **66**, 1547 (2003).

² J. L. Tallon and J. W. Loram, Physica C **349**, 53 (2001).

³ T. Timusk and B. Statt, Rep. Prog. Phys. **62**, 61 (1999).

⁴ A. Kaminski, S. Rosenkranz, H. M. Fretwell, J. C. Campuzano, Z. Li, H. Raffy, W. G. Cullen, H. You, C. G. Olson, C. M. Varma, and H. Höchst, Nature **416**, 610 (2002).

⁵ V. J. Emery and S. A. Kivelson, Nature **374**, 434 (1995).

⁶ C. M. Varma, Phys. Rev. B **55**, 14554 (1997).

⁷ C. M. Varma, Phys. Rev. B **73**, 155113 (2006).

⁸ S. Chakravarty, R. B. Laughlin, D. K. Morr, and C. Nayak, Phys. Rev. B **63**, 094503 (2001).

⁹ S. V. Borisenko, A. A. Kordyuk, A. Koitzsch, T. K. Kim, K. A. Nenkov, M. Knupfer, J. Fink, C. Grazioli, S. Turchini, and H. Berger, Phys. Rev. Lett. **92**, 207001 (2004).

- ¹⁰ B. Fauqué, Y. Sidis, V. Hinkov, S. Pailhès, C. T. Lin, X. Chaud, and P. Bourges, *Phys. Rev. Lett.* **96**, 197001 (2006).
- ¹¹ H. A. Mook, Y. Sidis, B. Fauqué, V. Balédent, and P. Bourges, *Phys. Rev. B* **78**, 020506 (2008).
- ¹² Y. Li, V. Balédent, N. Barišić, Y. Cho, B. Fauqué, Y. Sidis, G. Yu, X. Zhao, P. Bourges, and M. Greven, *Nature* **455**, 372 (2008).
- ¹³ J. H. Brewer, in *Encyclopedia of Applied Physics*, Vol. 11 (VCH Publishers, New York, 1994); A. Yaouanc and P. Dalmas de Reotier, *Muon Spin Rotation, Relaxation, and Resonance* (Oxford University Press, 2011).
- ¹⁴ J. E. Sonier, J. H. Brewer, R. F. Kiefl, R. I. Miller, G. D. Morris, C. E. Stronach, J. S. Gardner, S. R. Dunsiger, D. A. Bonn, W. N. Hardy, R. Liang, and R. H. Heffner, *Science* **292**, 1692 (2001).
- ¹⁵ J. E. Sonier, J. H. Brewer, R. F. Kiefl, R. H. Heffner, K. F. Poon, S. L. Stubbs, G. D. Morris, R. I. Miller, W. N. Hardy, R. Liang, D. A. Bonn, J. S. Gardner, C. E. Stronach, and N. J. Curro, *Phys. Rev. B* **66**, 134501 (2002).
- ¹⁶ G. J. MacDougall, A. A. Aczel, J. P. Carlo, T. Ito, J. Rodriguez, P. L. Russo, Y. J. Uemura, S. Wakimoto, and G. M. Luke, *Phys. Rev. Lett.* **101**, 017001 (2008).
- ¹⁷ A. Shekhter, L. Shu, V. Aji, D. E. MacLaughlin, and C. M. Varma, *Phys. Rev. Lett.* **101**, 227004 (2008).
- ¹⁸ C. Weber, T. Giamarchi, and C. M. Varma, *Phys. Rev. Lett.* **112**, 117001 (2014).
- ¹⁹ V. Scagnoli, U. Staub, Y. Bodenthin, R. A. de Souza, M. García-Fernández, M. Garganourakis, A. T. Boothroyd, D. Prabhakaran, and S. W. Lovesey, *Science* **332**, 696 (2011).
- ²⁰ O. E. Parfenov, A. A. Nikonov, and S. N. Barilo, *JETP Letters* **76**, 616 (2002).
- ²¹ V. G. Storchak, J. H. Brewer, D. G. Eshchenko, P. W. Mengyan, O. E. Parfenov, A. M. Tokmachev, P. Dosanjh, and S. N. Barilo, *J. Phys.: Conf. Ser.* **551**, 012024 (2014).
- ²² V. G. Storchak, O. E. Parfenov, J. H. Brewer, P. L. Russo, S. L. Stubbs, R. L. Lichti, D. G. Eshchenko, E. Morenzoni, T. G. Aminov, V. P. Zlomanov, A. A. Vinokurov, R. L. Kallagher, and S. von Molnár, *Phys. Rev. B* **80**, 235203 (2009).
- ²³ V. G. Storchak, O. E. Parfenov, J. H. Brewer, P. L. Russo, S. L. Stubbs, R. L. Lichti, D. G. Eshchenko, E. Morenzoni, V. P. Zlomanov, A. A. Vinokurov, and V. G. Bamburov, *Physica B* **404**, 899 (2009).
- ²⁴ V. G. Storchak, J. H. Brewer, D. J. Arseneau, S. L. Stubbs, O. E. Parfenov, D. G. Eshchenko, E. Morenzoni, and T. G. Aminov, *Phys. Rev. B* **79**, 193205 (2009).
- ²⁵ V. G. Storchak, J. H. Brewer, D. J. Arseneau, S. L. Stubbs, O. E. Parfenov, D. G. Eshchenko, and A. A. Bush, *Phys. Rev. B* **79**, 220406(R) (2009).
- ²⁶ V. G. Storchak, D. G. Eshchenko, E. Morenzoni, N. Ingle, W. Heiss, T. Schwarzl, G. Springholz, R. L. Kallagher, and S. von Molnar, *Phys. Rev. B* **81**, 153201 (2010).
- ²⁷ V. G. Storchak, J. H. Brewer, P. L. Russo, S. L. Stubbs, O. E. Parfenov, R. L. Lichti, and T. G. Aminov, *J. Phys: Cond. Matt.* **22**, 495601 (2010).
- ²⁸ V. G. Storchak, O. E. Parfenov, D. G. Eshchenko, R. L. Lichti, P. W. Mengyan, M. Isobe, and Yu. Ueda, *Phys. Rev. B* **85** 094406 (2012).
- ²⁹ V. G. Storchak, J. H. Brewer, D. G. Eshchenko, P. W. Mengyan, H. Zhou, and C. R. Wiebe, *J. Phys: Cond. Matt.* **25**, 115601 (2013).
- ³⁰ V. G. Storchak, J. H. Brewer, S. L. Stubbs, O. E. Parfenov, R. L. Lichti, P. W. Mengyan, J. He, I. Bredeson, D. Hitchcock, and D. Mandrus, *Phys. Rev. Lett.* **105**, 076402 (2010).
- ³¹ V. G. Storchak, J. H. Brewer, R. L. Lichti, T. A. Lograsso, and D. L. Schagel, *Phys. Rev. B* **83**, 140404(R) (2011).
- ³² B. Hitti, P. Birrer, K. Fischer, F. N. Gygax, E. Lippelt, H. Maletta, A. Schenck, and M. Weber, *Hyperf. Int.* **63**, 287 (1991).
- ³³ S. B. Sulaiman, S. Srinivas, N. Sahoo, F. Hagelberg, T. P. Das, E. Torikai, and K. Nagamine, *Phys. Rev. B* **49**, 9879 (1994).
- ³⁴ H. U. Suter, E. P. Stoll, and P. F. Meier, *Physica B* **326**, 329 (2003).
- ³⁵ W. Huang, V. Pacradouni, M. P. Kennett, S. Komiya, and J. E. Sonier, *Phys. Rev. B* **85**, 104527 (2012).
- ³⁶ B. Adiperdana, I. A. Dharmawan, R. E. Siregar, S. Sulaiman, M. I. Mohamed-Ibrahim, and I. Watanabe, *AIP Conf. Proc.* **1554**, 214 (2013).
- ³⁷ D. C. Johnston, *J. Magn. Magn. Mat.* **100**, 218 (1991).
- ³⁸ M. A. Kastner, R. J. Birgeneau, G. Shirane, and Y. Endoh, *Rev. Mod. Phys.* **70**, 897 (1998).
- ³⁹ O. Schärpf and H. Capellmann, *Z. Phys. B: Cond. Matt.* **80**, 253 (1990).
- ⁴⁰ T. Thio, T. R. Thurston, N. W. Preyer, P. J. Picone, M. A. Kastner, H. P. Jenssen, D. R. Gabbe, C. Y. Chen, R. J. Birgeneau, and A. Aharony, *Phys. Rev. B* **38**, 905 (1988).
- ⁴¹ M. Reehuis, C. Ulrich, K. Prokeš, A. Gozar, G. Blumberg, S. Komiya, Y. Ando, P. Pattison, and B. Keimer, *Phys. Rev. B* **73**, 144513 (2006).
- ⁴² A. S. Moskvin, *JETP Letters* **96**, 385 (2012).
- ⁴³ T. D. Stanescu and P. Phillips, *Phys. Rev. B* **69**, 245104 (2004).
- ⁴⁴ V. Aji and C. M. Varma, *Phys. Rev. B* **75**, 224511 (2007).
- ⁴⁵ Y. He and C. M. Varma, *Phys. Rev. Lett.* **106**, 147001 (2011).